

# Dilepton production and reaction dynamics in heavy-ion collisions at SIS energies from coarse-grained transport simulations

Stephan Endres,\* Hendrik van Hees, Janus Weil, and Marcus Bleicher

*Frankfurt Institute for Advanced Studies, Ruth-Moufang-Straße 1, D-60438 Frankfurt, Germany and*

*Institut für Theoretische Physik, Universität Frankfurt,*

*Max-von-Laue-Straße 1, D-60438 Frankfurt, Germany*

(Dated: May 22, 2015)

Dilepton invariant-mass spectra for heavy-ion collisions at SIS 18 and BEVALAC energies are calculated using a coarse-grained time evolution from the Ultra-relativistic Quantum Molecular Dynamics (UrQMD) model. The coarse-graining of the microscopic simulations enables to calculate thermal dilepton emission rates by application of in-medium spectral functions from equilibrium quantum-field theoretical calculations. The results show that extremely high baryon chemical potentials dominate the evolution of the created hot and dense fireball. Consequently, a significant modification of the  $\rho$  spectral shape becomes visible in the dilepton invariant-mass spectrum, resulting in an enhancement in the low-mass region  $M_{ee} = 200$  to  $600 \text{ MeV}/c^2$ . This enhancement, mainly caused by baryonic effects on the  $\rho$  spectral shape, can fully describe the experimentally observed excess above the hadronic cocktail contributions in Ar+KCl ( $E_{\text{lab}} = 1.76 \text{ AGeV}$ ) reactions as measured by the HADES collaboration and also gives a good explanation of the older DLS Ca+Ca ( $E_{\text{lab}} = 1.04 \text{ AGeV}$ ) data. For the larger Au+Au ( $E_{\text{lab}} = 1.23 \text{ AGeV}$ ) system, we predict an even stronger excess from our calculations. A systematic comparison of the results for different system sizes from C+C to Au+Au shows that the thermal dilepton yield increases stronger ( $\propto A^{4/3}$ ) than the hadronic background contributions, which scale with  $A$ , due to its sensitivity on the time evolution of the reaction. We stress that the findings of the present work are consistent with our previous coarse-graining results for the NA60 measurements at top SPS energy. We argue that it is possible to describe the dilepton results from SIS 18 up to SPS energies by considering the modifications of the  $\rho$  spectral function inside a hot and dense medium within the same model.

PACS numbers: 24.10.Lx, 25.75.Cj

Keywords: Monte Carlo simulations, Dilepton production

## I. INTRODUCTION

The study of dilepton production has for long been proposed as a good method to probe the change of hadronic properties in the hot and dense matter created in heavy-ion collisions and also as a possible observable for the creation of a deconfined phase at sufficiently high collision energies [1–4]. In contrast to the vacuum situation, a hadron can not only decay in a hot and dense medium but also interact with the constituents of the medium in scattering processes and resonance excitation. Many theoretical efforts have been undertaken over the last years to gain a better understanding of the in-medium properties of vector mesons [5–8]. The behavior of hadrons is of immanent interest for a full understanding of the phase structure given by Quantum Chromodynamics (QCD). One much-discussed aspect here is the change of the symmetries of QCD which is expected when going from the vacuum to finite temperature and finite baryochemical potential, especially the predicted restoration of chiral symmetry [9, 10]. Unlike all hadronic observables, which only provide information on the final freeze-out stage of the system, dileptons are not subject to strong interactions and consequently escape the fireball unscathed.

However, this also means that lepton pairs from all stages of the reaction will reach the detector. Especially for a theoretical description this is a big challenge, as it demands a realistic description of the whole space-time evolution of the heavy-ion reaction and taking the various dilepton sources into account.

On the experimental side several groups have undertaken the challenging task to measure dilepton spectra in heavy-ion collisions and thereby constrain the theoretical predictions. At SPS energies the NA60 Collaboration was able to measure the  $\rho$  in-medium spectral function for the first time, thanks to the high precision of the measurement [11]. The results were in line with previous CERES results [12] and found an excess in the invariant mass range from  $0.2$  to  $0.6 \text{ GeV}/c^2$ . This excess can be explained by a broadening of the  $\rho$  meson inside the hot and dense medium with small mass shifts [13–16]. At RHIC, these investigations were extended to even higher collision energies with basically the same results except for less dominant baryonic effects and a larger fraction of dileptons stemming from the QGP [17, 18].

Still more challenging is the interpretation of the dilepton measurements, which were performed in the low-energy regime at SIS 18 and BEVALAC. For collision energies around  $E_{\text{lab}} \approx 1 - 2 \text{ AGeV}$ , which will be in the focus of the present study, the DLS Collaboration measured a large excess beyond the results of theoretical microscopic calculations several years ago [19]. This

---

\* endres@th.physik.uni-frankfurt.de

disagreement between experiment and theory was called the “DLS puzzle”. In consequence, it triggered further experimental and theoretical investigations. Recently, the HADES experiment confirmed the former DLS results with a higher precision [20–23]. Although the theoretical microscopic models have been largely improved and extended since this time [24–29], a full and unambiguous description of the data has not yet been found. A satisfying answer is complicated by the fact that at such low energies a large number of processes contributes to the dilepton production, for which many parameters (like cross-sections, branching ratios, etc.) are not well-known. In addition interference effects are posing serious problems for transport Monte-Carlo simulations based on the evolution of phase-space densities. Here future measurements, for example in pion induced reactions as conducted by HADES, could give better constraints for the various parameters and reduce the uncertainty of the different contributions [30]. In any case, a full description of in-medium effects via off-shell dynamics or multi-particle interactions at high densities remains a difficult task, although some investigations on these issues have been conducted successfully [25, 31–37].

Besides the microscopic transport models, there exist also macroscopic approaches describing the evolution of the heavy-ion collision in terms of its thermodynamic properties. At high collision energies, i.e. at SPS or RHIC, a thermal calculation of dilepton emission is often applied, where a fireball expansion or a hydrodynamic calculation is used to model the bulk evolution of the system, while the dilepton emission is calculated using spectral functions at a given  $T$  and  $\mu_B$  [13, 15, 38–40]. But this approach works only if the collision energy is high enough. The application at  $E_{\text{lab}} \approx 1\text{-}2 \text{ AGeV}$  is hardly reliable.

However, there are no reasons why a macroscopic description of the reaction dynamics should not be possible at SIS 18 and BEVALAC energies, provided one can extract realistic values of energy and baryon density and, in consequence, temperature and baryochemical potential. On the contrary, due to the the expected high values of the baryon chemical potential, a study of the thermal properties of the system and the influence on the spectral shape of vector mesons might be very instructive. In the present work we argue that it is possible to obtain realistic values of  $T$  and  $\mu_B$  from microscopic calculations, provided one uses a large ensemble of events and averages over them (i.e. one “coarse-grains” the results) to obtain a locally smooth phase-space distribution. This ansatz, which was first presented and applied for the calculation of dilepton and photon spectra in [41], constitutes a compromise between (non-equilibrium) microscopic transport simulations and the calculation of dilepton emission with (equilibrium) spectral functions.

The same model was described in detail in [16] and already successfully applied to investigate dilepton production at SPS energies [42, 43]. The ansatz is used basically unchanged for the present low-energy study. The

only important extension is the implementation of the in-medium spectral function for the  $\omega$  meson. While for the NA60 results the cocktail contribution of the  $\omega$  was already subtracted from the thermal dilepton spectra, for comparing our calculations to the experimental HADES and DLS results a full description of the  $\omega$  contribution is required. Furthermore, the high baryon densities and slow evolution of the system increase the significance of its medium modifications at the energies considered here.

Note that we focus the present investigation on the larger systems Ar+KCl and Au+Au, where local thermalization can be assumed due to the size of the hot and dense fireball. For the smaller C+C system, which was also studied by HADES and DLS (in nearly minimum bias reactions), one finds that the average number of NN-collisions is so small that the assumption of a local thermalization is questionable. Furthermore, the experimental results indicate that the C+C dilepton spectra can be interpreted as the superposition of the underlying p+p and p+n collisions without any significant in-medium effects [22]. (However, when studying the effect of the system size on the dilepton production we will also consider central C+C collisions later on for completeness.)

This paper is organized as follows. Section II gives an introduction to the model and an overview of the different contributions considered for the calculation. Section III then presents the results for the thermodynamic evolution of the reaction (Sec. III A) and the resulting dilepton spectra (Sec. III B), furthermore the effect of the system size and fireball lifetime on the thermal dilepton yield is studied (Sec. III C). Finally, conclusions are drawn and an outlook to future studies is given in section IV.

## II. THE MODEL

The full theoretical description of the dilepton spectra requires to consider a large number of different production processes. At SIS energies, all dileptons stem from hadronic sources, in contrast to the situation at SPS, RHIC or LHC energies, where a significant contribution is assumed to come from  $q\bar{q}$ -annihilation in the quark-gluon plasma [44]. In general one can distinguish between two different hadronic contributions, such from long-lived particles (especially  $\pi$  and  $\eta$  mesons) and those from the short-lived light vector mesons (mainly  $\rho$ , but also  $\omega$  and  $\phi$ ). The former have a life time which is significantly larger than the duration of the hot and dense stage in a heavy-ion collision. Consequently, almost all of the decays of the long-lived mesons into lepton pairs will happen in the vacuum, i.e., no modification of the spectral shape is expected for those contributions. In contrast the latter mesons have a short life time and will therefore decay to a significant amount inside the fireball and their spectral properties are altered by the medium.

These differences are also significant for our approach. For the  $\pi$  and  $\eta$  meson contribution it is neither nec-

essary nor adequate to calculate thermal dilepton emission. The yields of these hadrons are determined directly from calculations with the UrQMD transport approach. For the  $\rho$  and the  $\omega$ , however, we calculate the thermal emission from coarse-grained transport simulations by application of in-medium spectral functions. Here the influence of the space-time evolution of the fireball is immanent, as the spectral shape will largely depend on the values of temperature  $T$  and baryon chemical potential  $\mu_B$ . Although for the  $\phi$  some medium-modifications of the spectral shape are predicted as well, we here skip a full thermal calculation for the present investigation. On the one hand,  $\phi$  production is strongly suppressed at the low energies considered here and will therefore hardly give any significant contribution to the invariant mass spectrum, on the other hand the predicted medium effects are rather small. Consequently, the  $\phi$  contribution is directly extracted from the UrQMD calculations, as applied for the  $\pi$  and  $\eta$ . At higher invariant dilepton masses, i.e. mainly above  $1 \text{ GeV}/c^2$ , also multi-pion states in form of broad resonances influence the dilepton production. This contribution is also calculated as thermal emission.

The underlying model for all our considerations is the Ultra-relativistic Quantum Molecular Dynamics approach (UrQMD), which is a non-equilibrium cascade model [45–48]. It includes all relevant hadronic resonances up to a mass of  $2.2 \text{ GeV}/c^2$ . The model gives an effective solution to the Boltzmann equation. The hadrons are propagated on classical trajectories and can interact in form of elastic and inelastic scatterings. Production of new particles via resonance formation (e.g.,  $\pi + \pi \rightarrow \rho$ ) or the decay of resonances in form of  $\Delta \rightarrow N + \pi$ . String excitation is possible for hadron-hadron collisions with  $\sqrt{s} > 3 \text{ GeV}$  but is negligible in the SIS energy regime considered here.

### A. Coarse-Grained Contributions

For the calculation of thermal emission rates by applying in-medium spectral functions, one needs to extract the local thermodynamic properties from the UrQMD simulations. To obtain a phase-space distribution that is sufficiently smooth in a small volume  $\Delta V$  around each point in space-time, we simulate a large ensemble of events. A grid of space-time cells with  $\Delta x = \Delta y = \Delta z = 0.7 - 0.8 \text{ fm}$  and  $\Delta t = 0.6 \text{ fm}/c$  is set up and the energy-momentum tensor  $T_{\mu\nu}$  as well as the net-baryon four-flow  $j_\mu^B$  are determined in each of these cells as

$$T^{\mu\nu} = \int d^3p \frac{p^\mu p^\nu}{p^0} f(\vec{x}, \vec{p}, t) = \frac{1}{\Delta V} \left\langle \sum_{i=1}^{N_h \in \Delta V} \frac{p_i^\mu \cdot p_i^\nu}{p_i^0} \right\rangle, \\ j_\mu^B = \int d^3p \frac{p^\mu}{p^0} f_B(\vec{x}, \vec{p}, t) = \frac{1}{\Delta V} \left\langle \sum_{i=1}^{N_B \in \Delta V} \pm \frac{p_i^\mu}{p_i^0} \right\rangle. \quad (1)$$

The rest frame according to Eckart [49] can be found by performing a Lorentz boost such that the baryon flow vanishes in the cell, i.e.  $\vec{j}_B = 0$ . In the Eckart frame we extract the energy density  $\epsilon$  and baryon density  $\rho_B$  as an input to obtain the temperature  $T$  and baryon chemical potential  $\mu_B$  by applying an equation of state. At SIS energies it is sufficient to use a hadron-resonance gas (HG-EoS) [50]. This HG-EoS includes the same degrees of freedom as the UrQMD model.

It is important to bear in mind that the procedure as described above assumes local (isotropic) equilibrium in the cell. In macroscopic descriptions of heavy-ion collisions kinetic and chemical equilibrium is usually introduced as an ad-hoc assumption. However, we extract the thermal properties from a transport (i.e. non-equilibrium) approach which has effects as viscosity and heat conduction. Although the creation of an approximately equilibrated stage is usually considered to happen on extremely short time scales after the beginning of the collision, it is difficult to prove the creation of thermal and chemical equilibrium explicitly. Previous studies comparing UrQMD calculations with the results from the statistical thermal model showed that it might take up to 8–10 fm/c before one can assume the system to be in approximate kinetic and chemical equilibrium on a global scale [51, 52]. For practical reasons we use the momentum-space anisotropy to characterize to which degree the local kinetic equilibrium is constituted in the present study. Here, the coarse-grained microscopic transport calculations show a significant deviation from equilibrium in form of large pressure differences between the longitudinal and transverse components of the energy momentum tensor at the beginning of the reaction: During the first few fm/c the longitudinal pressure is significantly larger than the transverse pressures, which is mainly due to the deposition of high longitudinal momenta from the colliding nuclei. It has been suggested that in this case one can determine realistic values for the energy density by using a generalized equation of state [53, 54] where

$$\varepsilon_{\text{real}} = \frac{\varepsilon}{r(x)}. \quad (2)$$

For a system with Boltzmann-type pressure anisotropies the relaxation function  $r(x)$  takes the form

$$r(x) = \begin{cases} \frac{x^{-1/3}}{2} \left( 1 + \frac{x \operatorname{artanh} \sqrt{1-x}}{\sqrt{1-x}} \right) & \text{for } x \leq 1 \\ \frac{x^{-1/3}}{2} \left( 1 + \frac{x \operatorname{arctan} \sqrt{x-1}}{\sqrt{x-1}} \right) & \text{for } x \geq 1 \end{cases}, \quad (3)$$

where  $x = (P_{||}/P_{\perp})^{3/4}$  denotes the pressure anisotropy. With this result we can extract meaningful energy densities from the coarse-grained distributions also in the very early stage of the reaction, as has already been shown in [16].

With the values of  $T$  and  $\mu_B$  known for all cells, the calculation of the thermal dilepton emission is straight-

forward [7, 55] and takes the form

$$\frac{dN_{ll}}{d^4x d^4q} = -\frac{\alpha_{\text{em}}^2 L(M)}{\pi^3 M^2} f^B(q \cdot U; T) \times \text{Im} \Pi_{\text{em}}^{(\text{ret})}(M, \vec{q}; \mu_B, T) \quad (4)$$

with the Bose distribution function  $f^B$  and the lepton phase-space  $L(M)$ , while  $M$  and  $q$  denote the invariant mass and the momentum of the lepton pair, respectively, and  $\alpha_{\text{em}}$  is the electromagnetic coupling constant. The relevant physical quantity is the retarded electromagnetic current-current correlator  $\Pi_{\text{em}}^{(\text{ret})}$  which contains all the information on the medium effects of the spectral function.

Note that equation (4) is derived for the case of full chemical equilibrium, which requires all chemical potentials of non-conserved charges to be zero. Similar to the kinetic anisotropies at the beginning of the reaction, also deviations from the chemical equilibrium composition of the system appear at the early stages of transport simulations. Especially an overpopulation of pions is observed here, which dominates the evolution for a significant period of time [56]. The appearance of a finite pion chemical potential  $\mu_\pi$  was explained by the large initial production of pions and their long relaxation time [57, 58]. This is of particular importance for the present study since a finite chemical potential  $\mu_\pi$  was considered to have a significant influence on the thermal dilepton emission rates by its influence on the  $\pi$ - $\rho$  interactions [59, 60]. For the present calculations, we extract the pion chemical potential in Boltzmann approximation for each cell and consider its effect on the thermal dilepton emission (i) in form of its direct influence on the spectral functions and (ii) as additional fugacity factor, which will show up in equation (4) for the chemical non-equilibrium case.

In the following the different thermal contributions which are considered for the present study are discussed.

### 1. Thermal $\rho$ and $\omega$ Emission

Several approaches for the description of in-medium effects on vector mesons exist. However, a full description of the different effects that influence the spectral shape in a hot and dense medium are highly non-trivial, and there are only a few calculations that include both the effects of finite temperature and density. E.g. in Ref. [61] the in-medium spectral functions were determined using empirical scattering amplitudes. However, this spectral function is calculated in low-density approximation for a weakly interacting pion-nucleon gas and tested only up to densities of  $2\rho_0$ . The application of this approach is therefore questionable for the situation at SIS energies where very high net baryon densities are reached.

In the present work a calculation from hadronic many-body theory [62–65] is applied, which has proven to successfully describe the dilepton spectra at SPS and RHIC energies [14, 66]. In the medium, three different contribu-

tions to the self-energy of the  $\rho$  are taken into account here. These are

- (a) the modification of the pion cloud of the  $\rho$  meson by particle-hole and  $\Delta$ -hole excitations in the medium,
- (b) scattering with mesons ( $M = \pi, K, \bar{K}, \rho$ ) and
- (c) scattering with the most abundant baryon resonances ( $B = N, \Delta_{1232}, N_{1440}^*, \dots$ ).

The in-medium propagator consequently takes the form

$$D_\rho = \frac{1}{M^2 - m_\rho^2 - \Sigma_{\rho\pi\pi} - \Sigma_{\rho M} - \Sigma_{\rho B}}. \quad (5)$$

The  $\omega$  spectral function [66] is similarly constructed. However, here the situation is more complicated as the  $\omega$  is basically a three-pion state, and the vacuum self energy is given by decays into  $\rho\pi$  or  $3\pi$ . The full in-medium propagator reads

$$D_\omega = [M^2 - m_\omega^2 + i m_\omega (\Gamma_{3\pi} + \Gamma_{\rho\pi} + \Gamma_{\omega\pi\rightarrow\pi\pi}) - \Sigma_{\omega\pi b_1} - \Sigma_{\omega B}]^{-1}. \quad (6)$$

It includes the following contributions:

- (a)  $\omega \rightarrow \rho\pi$  decays including the corrections from the medium-modified  $\rho$  spectral function,
- (b) the direct  $\omega \rightarrow 3\pi$  decays,
- (c)  $\omega\pi \rightarrow \pi\pi$  inelastic scattering,
- (d)  $\omega\pi \rightarrow b_1$  resonance scattering and
- (e)  $\omega N \rightarrow N_{(1520)}, N_{(1650)}$  resonance scattering at an effective nucleon density  $\rho_{\text{eff}}$ .

To take into account the off-equilibrium of the pions an additional fugacity factor is introduced in equation (4), as already explained above. In one-loop approximation, for the thermal  $\rho$  and  $\omega$  emission one obtains an additional overall fugacity factor [7]

$$z_\pi^n = e^{n\mu_\pi/T}. \quad (7)$$

The exponent  $n$  hereby takes the value 2 in case of the  $\rho$  emission and 3 for the  $\omega$  contribution [13]. The final yield is then calculated according to

$$\frac{dN_{e^+e^-}}{dM} = \Delta x^4 \int \frac{d^3p}{p_0} \frac{dN_{e^+e^-}}{d^4x d^4p} z_\pi^n. \quad (8)$$

Note that the four-volume  $\Delta x^4 = \Delta t \Delta V$  of the cell is an invariant quantity and therefore the same in all reference frames.

As it is not reasonable or possible to calculate thermal dilepton emission for all cells (e.g., due to low temperature) we also include a non-thermal (“freeze-out”) contribution for the  $\rho$  and  $\omega$  meson. Those dileptons are directly extracted from the UrQMD calculations (for details see section II B 3).

## 2. Multi- $\pi$ Contribution

Although it is known from previous theoretical investigations at higher collision energies that the multi-pion contribution plays a significant role only for masses greater than  $1 \text{ GeV}/c^2$ , which is mostly beyond the kinematic limit of dilepton production at SIS energies, we include this contribution for completeness. Here the same description as developed in [13, 14] is applied which uses chiral reduction techniques for the case of the chiral limit [67]. This leads to a chiral mixing of the isovector part of the vector and axial-vector correlators. The isovector-vector current correlation function takes the form

$$\begin{aligned} \Pi_V(p) = & (1 - \hat{\varepsilon}) z_\pi^4 \Pi_{V,4\pi}^{\text{vac}} + \frac{\hat{\varepsilon}}{2} z_\pi^3 \Pi_{A,3\pi}^{\text{vac}} \\ & + \frac{\hat{\varepsilon}}{2} (z_\pi^4 + z_\pi^5) \Pi_{A,5\pi}^{\text{vac}}, \end{aligned} \quad (9)$$

where  $\hat{\varepsilon}$  denotes the mixing parameter which depends on temperature, critical temperature and the pion chemical potential. The result is an admixture of three-pion and five-pion axial-vector pieces on the vector four-pion part. Once again, as in case of the  $\rho$  and  $\omega$  spectral functions, the effect of a finite pion chemical potential also enters in form of a fugacity factor  $z_\pi^n$  with  $n = 3, 4, 5$  denoting the pion multiplicity of the corresponding state. Note that the two-pion and the three-pion piece corresponding to the decay  $a_1 \rightarrow \rho + \pi$  are already included in the  $\rho$  spectral function and are therefore not considered for the multi-pion contribution.

## B. Transport Contributions

### 1. $\pi$ and $\eta$ Dalitz Decay

The  $\pi^0$  and the  $\eta$  pseudo-scalar mesons can both decay into a lepton pair via the Dalitz decays

$$\pi^0 \rightarrow \gamma l^+ l^-, \quad \eta \rightarrow \gamma l^+ l^-. \quad (10)$$

Following the scheme presented in [27], we treat this decay as a two-step process: First the decay of the pseudo-scalar meson into a photon  $\gamma$  and a virtual photon  $\gamma^*$  and the following electromagnetic conversion of the  $\gamma^*$  into a lepton pair [68]. The width of the meson decaying into a photon and a virtual photon can be related to the radiative decay width. The full expression then takes the form

$$\begin{aligned} \frac{d\Gamma_{M \rightarrow \gamma l^+ l^-}}{dM^2} = & 2\Gamma_{M \rightarrow 2\gamma} \left(1 - \frac{M^2}{m_M^2}\right)^3 \\ & \times |F_{M\gamma\gamma^*}(M^2)|^2 \frac{\alpha_{em}}{3\pi M^2} L(M). \end{aligned}$$

With the lepton phase space  $L(M)$  and the form factor  $F_{M\gamma\gamma^*}(M^2)$ . Here we use the form factors as obtained from fits to experimental data, which are in very good

agreement with the values as predicted by the Vector Dominance Model [68]:

$$\begin{aligned} F_{\pi^0\gamma\gamma^*}(M^2) &= 1 + b_{\pi^0} M^2, \\ F_{\eta\gamma\gamma^*}(M^2) &= \left(1 - \frac{M^2}{\Lambda_\eta^2}\right)^{-2}, \end{aligned} \quad (11)$$

with  $b_{\pi^0} = 5.5 \text{ GeV}^{-2}$  and  $\Lambda_\eta = 0.72 \text{ GeV}$ . Note that for this contribution, we only consider those particles from the final freeze-out of the calculation, neglecting all  $\pi$  and  $\eta$  which are reabsorbed during the evolution of the collision.

### 2. $\phi$ Direct Decay

The width for the direct decays of the vector mesons can be determined via [69]

$$\Gamma_{V \rightarrow ll}(M) = \frac{\Gamma_{V \rightarrow ll}(m_V)}{m_V} \frac{m_V^4}{M^3} L(M). \quad (12)$$

For the branching ratio at the meson pole mass  $m_V$  we use the value from the particle data group,  $\Gamma_{\phi \rightarrow ee}(m_V)/\Gamma_{\text{tot}} = 2.95 \cdot 10^{-4}$  [70].

An important difference compared to the procedure for the long-lived pseudo-scalar mesons is the assumption that the  $\phi$  mesons continuously emit dileptons over their lifetime [71]. That means, we track the time of production and the decay (or absorption) of the  $\phi$  and integrate over the corresponding lifetime in the particle's rest frame.

$$\frac{dN_{ll}}{dM} = \frac{\Delta N_{ll}}{\Delta M} = \sum_{i=1}^{N_{\Delta M}} \sum_{j=1}^{N_\rho} \int_{t_i}^{t_f} \frac{dt}{\gamma_V} \frac{\Gamma_{V \rightarrow ll}(M)}{\Delta M}. \quad (13)$$

The factor  $\gamma_V$  is here introduced to account for the relativistic time dilation in the computational frame compared to the vector mesons rest frame.

This “shining approach” is identical with the assumption of simply having one additional dilepton from each  $\phi$  (weighted with the according branching ratio) if there is no absorption. But inside a dense medium, there is a significant chance that the particle will not decay but suffer an inelastic collision. Therefore the probability for the decay into a dilepton is reduced, and the shining as described above accounts for this effect [72].

### 3. Non-thermal $\rho$ and $\omega$

There are two situations, where a thermal calculation of the dilepton emission from spectral functions becomes difficult or even unreasonable. Firstly, for cells with no baryon content, where the Eckart definition of the rest-frame does not apply (those cells are found in the late stage of the reaction in very peripheral cells) and secondly for cells where the temperature is found to be below 50 MeV. In the latter case, when going to such usually

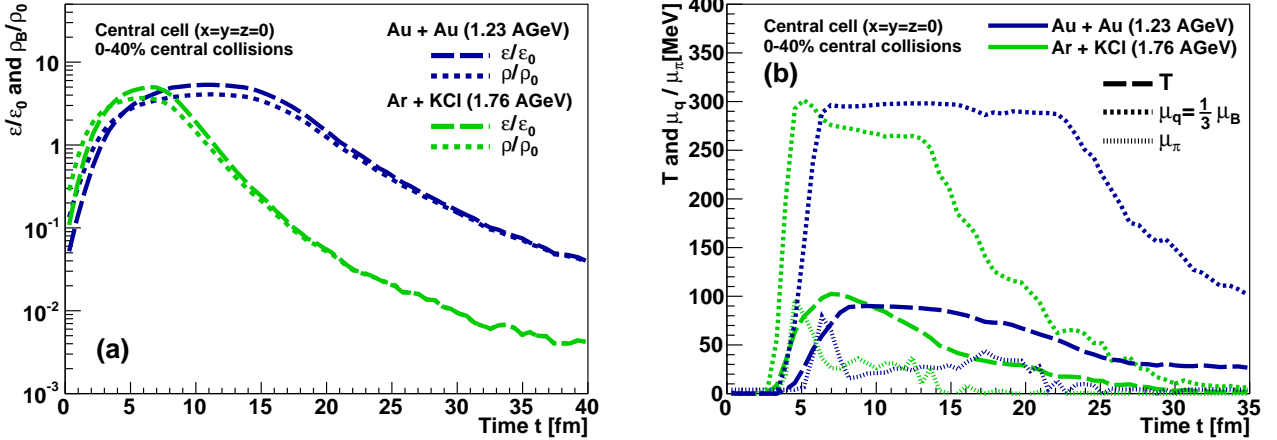


Figure 1. (Color online) Time evolution of the energy and baryon densities  $\varepsilon$  and  $\rho$  in units of the according ground-state densities (a) and for temperature  $T$  as well as the baryon and pion chemical potential,  $\mu_B$  respectively  $\mu_\pi$  (b) for the central cell (i.e., at  $x = y = z = 0$ ). The results as obtained via coarse-graining of microscopic transport calculations are shown for Ar+KCl collisions at  $E_{\text{lab}} = 1.76$  AGeV and for Au+Au reactions at 1.23 AGeV.

low-density cells, the determination of  $T$  and  $\mu_B$  becomes less accurate and one will necessarily come to the point where the assumption of a thermalized system in the cell becomes unreliable. Consequently, we do not assume any thermal dilepton emission here. This procedure is in line with the findings of thermal-model studies [73], where it was shown that the freeze-out temperature in heavy-ion collisions at  $E_{\text{lab}} = 1 - 2$  AGeV is around 50 MeV. This also indicates that it is neither necessary nor suggestive to assume thermalization of the system at lower temperatures.

However, one has to consider that dilepton emission from  $\rho$  and  $\omega$  mesons is of course also possible in the cells for which one of the conditions mentioned above pertains. As the macroscopic picture is questionable here, we apply a similar procedure as for the  $\phi$  (described in section II B 2) to extract the dilepton emission from the microscopic simulation. The width for the direct decays of the vector mesons can likewise be determined via equation (12). For the branching ratio at the meson-pole mass we use the values from the particle data group, i.e.  $\Gamma_{\rho \rightarrow ee}/\Gamma_{\text{tot}} = 4.72 \cdot 10^{-5}$  and  $\Gamma_{\omega \rightarrow ee}/\Gamma_{\text{tot}} = 7.28 \cdot 10^{-5}$  [70]. However, the  $\omega$  can not only decay into a lepton pair directly, but also via Dalitz conversion into a pseudo-scalar meson and a dilepton. As in the case of the  $\pi$  and the  $\eta$  equation (11) applies here. Only the form factor is different and takes the form

$$|F_\omega(M^2)|^2 = \frac{\Lambda_\omega^2 (\Lambda_\omega^2 + \gamma_\omega^2)}{(\Lambda_\omega^2 - M^2) + \Lambda_\omega^2 \gamma_\omega^2} \quad (14)$$

with the parameters  $\Lambda_\omega = 0.65$  GeV and  $\gamma_\omega = 0.04$  GeV [27, 74].

Similarly to the procedure for the  $\phi$  meson, a continuous emission of dileptons from the  $\rho$  and  $\omega$  is assumed in these special cases. However, as we consider space-time

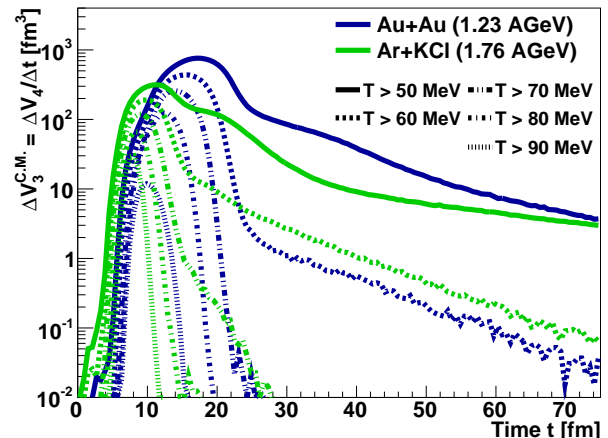


Figure 2. (Color online) Time evolution of the thermal volume  $V_3^{\text{C.M.}}$  as seen from the center-of-momentum frame of the collision. This is equal to the thermal four-voulume  $V_4$  for each timestep divided by the length of  $\Delta t$ , which is 0.6 fm/c here. The results are shown for Ar+KCl collisions at  $E_{\text{lab}} = 1.76$  AGeV and for Au+Au reactions at 1.23 AGeV as obtained via coarse-graining of microscopic transport calculations. The results are plotted for different temperatures.

cells with a definite length of the time-steps  $\Delta t$ , the dilepton rate is multiplied with this time instead of the actual particle's lifetime within the cascade simulation. This is done to guarantee consistency, avoid double counting and strictly distinguish between cells with thermal and non-thermal emission. Consequently, here equation (13)

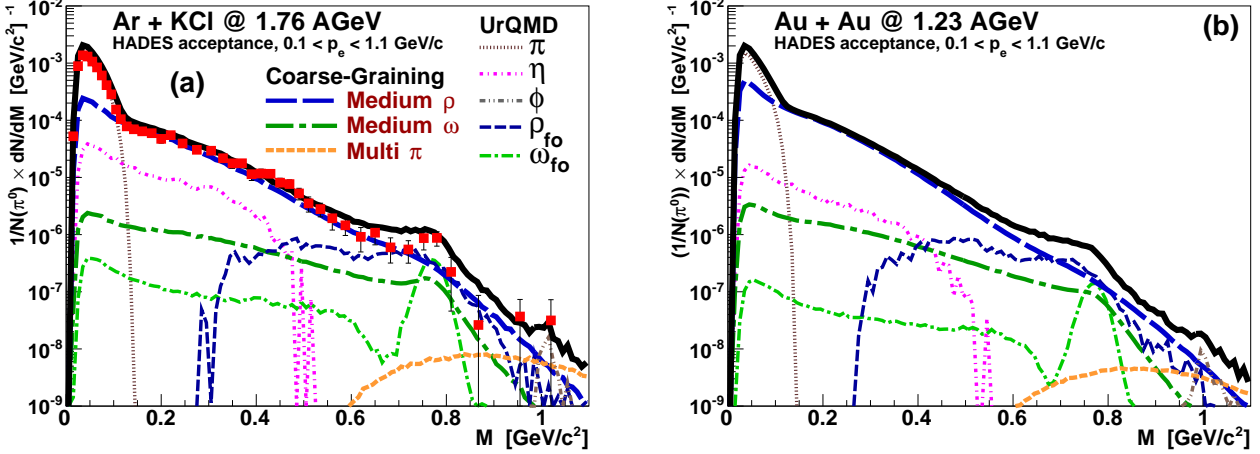


Figure 3. (Color online) Invariant mass spectra of the dielectron yield for Ar+KCl collisions at  $E_{\text{lab}} = 1.76$  AGeV (a) and for Au+Au at  $E_{\text{lab}} = 1.23$  AGeV (b). The results are normalized to the average total number of  $\pi^0$  per event and shown within the HADES acceptance. The results for Ar+KCl are compared to the experimental data from the HADES Collaboration [23].

takes the form

$$\frac{dN_u}{dM} = \frac{\Delta N_u}{\Delta M} = \sum_{i=1}^{N_{\Delta M}} \sum_{j=1}^{N_V} \frac{\Delta t}{\gamma V} \frac{\Gamma_{V \rightarrow u}(M)}{\Delta M}, \quad (15)$$

and is applied for each time step  $\Delta t$ .

### III. RESULTS

For the results presented here we used calculations with an ensemble of 1000 UrQMD events. However, several runs using different UrQMD events as input had to be performed to obtain enough statistics especially for the non-thermal  $\rho$  and  $\omega$  contributions. Note that in case of the experimental Ar+KCl reaction we simulated the collision of two calcium ions instead, as this makes the calculation easier for symmetry reasons. Effectively it is the same as the Ar+K or Ar+Cl reactions that were measured in the experiment and the size of the system remains identical. To simulate the correct impact parameter distribution, we made a Woods-Saxon type fit to the HADES trigger conditions for Ar+KCl [75] and Au+Au [76]. In both cases this approximately corresponds to a selection of the 0-40% most central collisions. The number of  $\pi^0$  per event, which will be important for the normalization of the dilepton spectra, are found to agree well with the HADES measurement for Ar+KCl reactions. Here the HADES collaboration measured  $N_{\pi^0}^{\text{exp}} = 3.5$  where we find  $N_{\pi^0}^{\text{sim}} \approx 3.9$ , i.e. the deviation is only 12%. For the larger Au+Au system a number  $N_{\pi^0}^{\text{sim}} \approx 8.0$  results from the events generated with the UrQMD model. Note that for reasons of self-consistency we normalize the dilepton spectra with the UrQMD  $\pi^0$  yield, not the experimental one.

The final dilepton results were filtered with the HADES acceptance filter [77], and momentum cuts were applied to compare the simulations with the experimental results. As only very preliminary results and no filters are available for the Au+Au reactions at 1.23 AGeV, we used the same filter as for p+p and p+n reactions at 1.25 AGeV which should be quite close to the final acceptance [76].

In case of the DLS Ca+Ca spectrum, version 4.1 of the DLS acceptance filter [78] is used. Furthermore, an RMS smearing of 10% is applied to account for the detector resolution. For this reaction we used a minimum-bias simulation of Ca+Ca events, because impact-parameter distributions are not available for DLS. Here the final invariant-mass spectrum is normalized to the total cross-section of a Ca+Ca reaction.

#### A. Reaction Dynamics

The main difference between the two reactions considered here is the size of the colliding nuclei. Therefore, it is interesting to first have a look at the evolution of the reaction for both systems. In Fig. 1 the evolution of the baryon and energy density (a) as well as the evolution of temperature and the chemical potentials (b) are shown. Both figures show that the maximum values in the central cell of the grid, i.e., in the center of the collision, reach similar values up to roughly 5-8 times ground-state baryon density  $\rho_0$  and energy density  $\varepsilon_0$  for both systems. In case of the larger system (Au+Au) a plateau develops for a duration of more than 10 fm/c, while for Ar+KCl (respectively Ca+Ca in our simulations) the densities drop off rather quickly after reaching the maximum. Note that the values for the energy density  $\varepsilon$  shown in Fig. 1 are corrected for the pressure

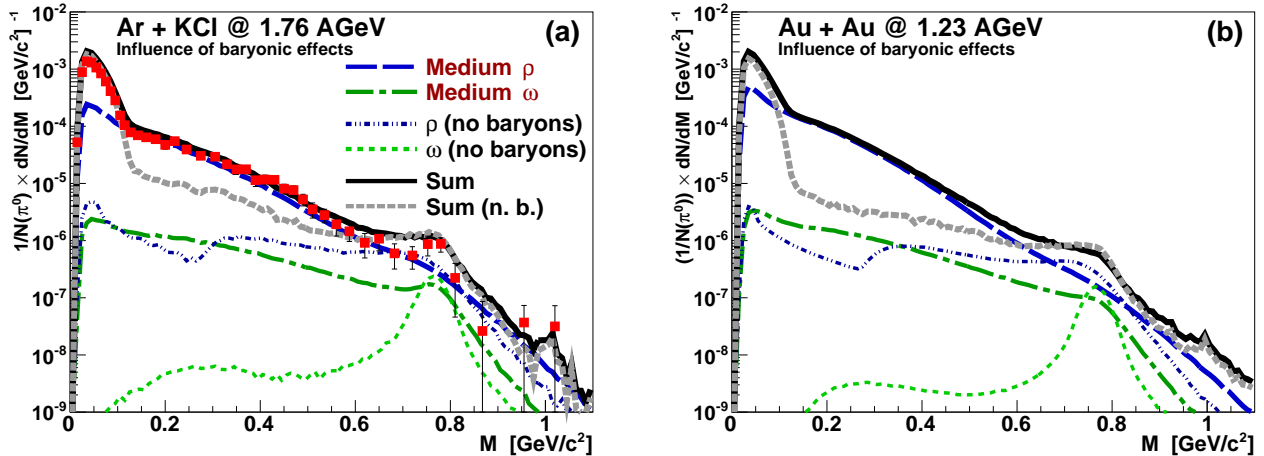


Figure 4. (Color online) Comparison of invariant mass spectra with the full spectral function and for the case of no baryonic effects (i.e. for  $\rho_{\text{eff}} = 0$ ). As in Fig. 3, the dielectron yields for Ar+KCl collisions at  $E_{\text{lab}} = 1.76$  AGeV (a) and for Au+Au at  $E_{\text{lab}} = 1.23$  AGeV (b) are shown within HADES acceptance and normalized to the average number of produced  $\pi^0$ . Note that the UrQMD contributions are included in the sum, but the different single yields are not shown explicitly for reasons of lucidity.

anisotropy at the beginning of the collision.

With regard to the evolution of temperature and baryochemical potential in Fig. 1 (b), we find that also here similar top values are obtained. In both reactions, Ar+KCl and Au+Au, we get peak values of  $T \approx 100$  MeV and  $\mu_B \approx 900$  MeV. (Note that the quark chemical potential  $\mu_q = \frac{1}{3}\mu_B$  is shown instead of the baryon chemical potential.) Especially the values of  $\mu_B$  are much higher here and show a different evolution than in our recent study for top SPS energy [16]. In case of Au+Au collisions the central cell stays for approximately  $20 \text{ fm}/c$  in a stage with extremely high baryochemical potential, so that any baryon-driven effect on the dilepton spectra should be clearly visible for this system. Similar findings are also true for Ar+KCl reactions, but with significantly shorter lifetime. The maximum temperature is approximately 10 MeV higher in the latter reaction due to the slightly higher collision energy.

The pion chemical potential rises up to values of around 100 MeV and then equally quickly drops to values around 20-50 MeV for the rest of the reaction. The peak at the beginning can be explained with the non-equilibrium nature of the cascade, where a large number of pions is produced rapidly at the very beginning before the system has time to equilibrate.

The corresponding evolution of the thermal four-volume at each time step, divided by its duration  $\Delta t$ , as obtained for both systems from the coarse-grained microscopic transport calculations is shown in Fig. 2. This quantity is the spatial volume for the different temperature ranges as seen from the center-of-momentum frame of the collision. One observes that the hotter cells created during the evolution of the system (for temperatures above 80 respectively 90 MeV) are present only for com-

paratively short time spans, and their number is significantly smaller than the volume of cells with lower temperatures. Even at the end of the reaction, one will still find a few cells at temperatures above 50 MeV. Note, however, that the dilepton emission from these late stage cells is marginal and insignificant with regard to the overall integrated dilepton spectra.

## B. Dilepton Spectra

### 1. HADES Results

The resulting dielectron invariant-mass spectra for the two heavy-ion reactions measured by the HADES Collaboration are presented in Fig. 3. The left figure (a) shows the Ar+KCl results at 1.76 AGeV compared to the experimental data and the right figure (b) shows our prediction for the larger Au+Au system at 1.23 AGeV (no dilepton data are published for the Au+Au measurement yet). The coarse-graining results for the Ar+KCl case show good agreement with the experimental data, especially the mass range between 0.2 and 0.6  $\text{GeV}/c^2$  can be well described within this approach. This is different from previous simulations which have indicated an excess of the experimental outcome above the cocktail respectively the transport calculations [23, 79, 80]. The dominant contribution stems from a broadened  $\rho$ . It is further noteworthy that also the  $\omega$  shows a non-negligible broadening in our model results. A slight overestimation of the experimental dilepton yield shows up for the low-mass region (below  $150 \text{ MeV}/c^2$ ) which is dominated by  $\pi$  Dalitz decays, an effect that also has been found in other transport calculations [79]. It remains unclear where this pion

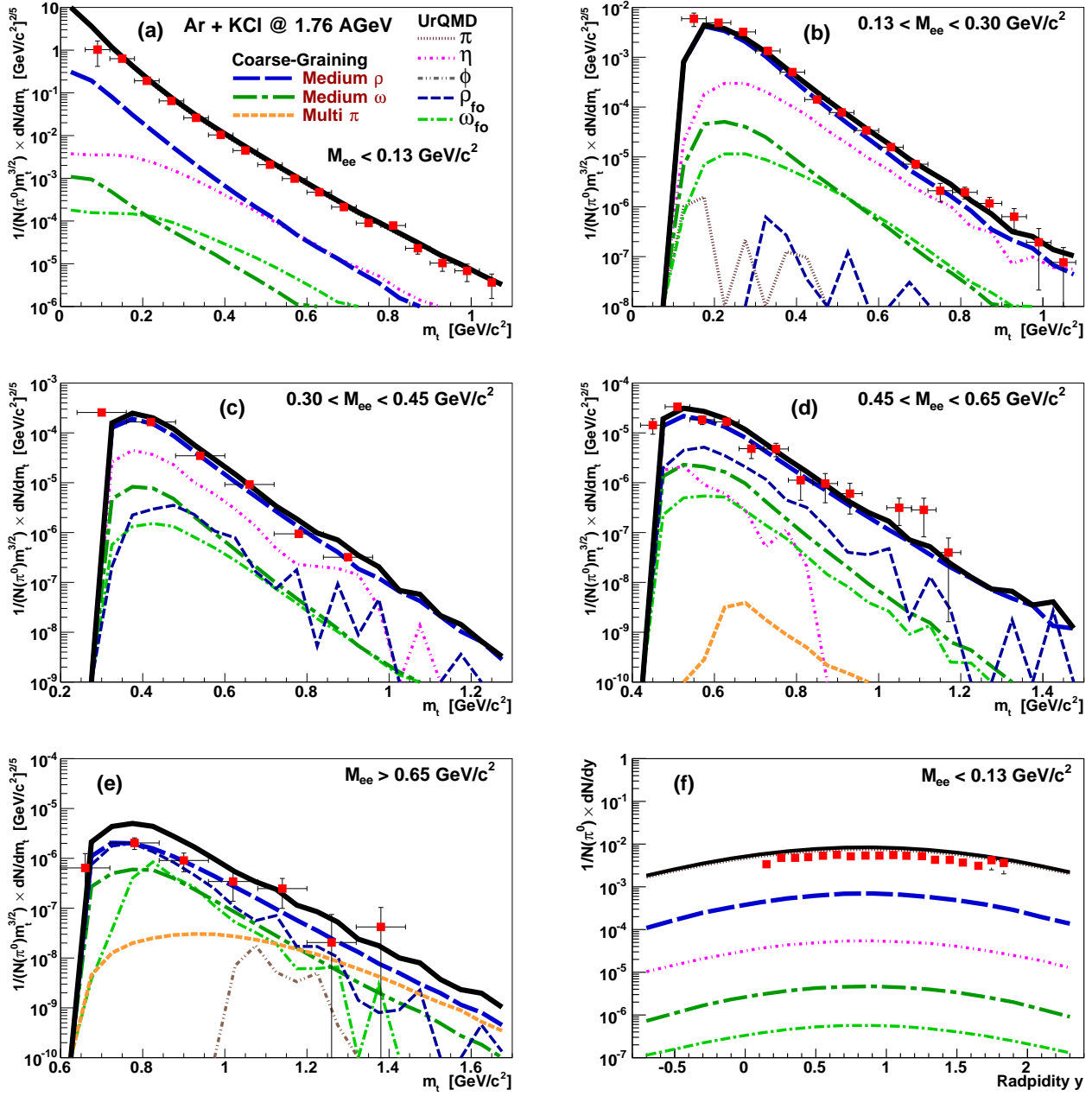


Figure 5. (Color online) Transverse-mass spectra of the dielectron yield in different mass bins (a)-(e) and the dielectron rapidity spectrum of pairs with invariant mass  $M_{ee} < 0.13 \text{ GeV}/c^2$  (f) for Ar+KCl collisions at  $E_{\text{lab}} = 1.76 \text{ AGeV}$ . The results are compared to the experimental data from the HADES Collaboration [23]. In contrast to Figures 3 and 4 the theoretical results here are not shown within the HADES acceptance, as these data are already fully corrected for acceptance and efficiency.

excess stems from. As the dielectron yield is normalized to the total  $\pi^0$  number, theory and experiment should agree in the pion-dominated mass-region. Therefore the deviation may be due to a phase-space effect, connected to the geometrical detector acceptance. Another slight excess of the model results is manifest around the pole mass of the  $\rho$ . A significant part of the dileptons here stems from non-thermal  $\rho$  mesons, which directly come from the UrQMD calculations using the shining method.

As for UrQMD the  $\rho$ -production cross sections in the threshold region are known to be slightly too large [80], this overestimation is probably due to the non-thermal contribution.

The medium effects become even stronger in the larger Au+Au system, as can be seen in the right part (b) of Fig. 3. The yield from the thermal  $\rho$  is higher at low masses compared to the Ar+KCl reaction and also the thermal  $\omega$  is slightly stronger here. This is in line with

the findings of the previous section III A, where it was pointed out that the hot and dense stage lives substantially longer in the Au+Au reaction. Consequently, the  $\rho$  contribution is larger for the Au+Au system as compared to the Ar+KCl reaction, especially at the low masses where the in-medium broadening comes into account.

The dramatic effect of the presence of baryonic matter on the dilepton spectra can be seen in Fig. 4. Here the thermal contributions to the  $e^+e^-$  invariant mass spectrum of the  $\rho$  and the  $\omega$  for the case that no baryons and anti-baryons are present (i.e. the effective baryon density  $\rho_{\text{eff}}$  is put to zero) are compared to the results with the full medium effects. The baryon-driven effects are significant, with the broadening around the pole mass of the  $\rho$  and  $\omega$  meson and the strong increase in the low-mass dilepton yield, which is again stronger for the larger Au+Au system as compared to Ar+KCl. Additionally the total sum for the two cases with and without baryonic effects is shown, including also all the UrQMD contributions (details are omitted for clarity). Here we find stronger differences between Ar+KCl and Au+Au, mainly due to the relatively smaller contribution from the  $\eta$  for Au+Au reactions, compared to the stronger broadening of the  $\rho$ .

Looking not only at the invariant-mass spectra but also at the transverse-momentum distributions in different mass bins in Fig. 5 (a)-(e), one finds again a good agreement of our model calculations with the HADES data for Ar+KCl. While for the lowest mass bin ( $M_{ee} < 0.13 \text{ GeV}/c^2$ ) the pion contribution dominates, the thermal  $\rho$  is the most significant contribution to the dileptons in all other bins. For the highest mass bin ( $M_{ee} > 0.65 \text{ GeV}/c^2$ ), which includes the pole mass region of the  $\rho$ , one can observe a slight overestimation of the total yield, similar to the one observed in the invariant mass spectrum in this mass region (see Fig. 3(a)). Once again, we argue that this is due to the high  $\rho$ -production cross section in the threshold region and therefore stems from the non-thermal transport  $\rho$ . As one can see, the thermal  $\rho$  alone would describe the data very well.

For the lowest mass bin, the HADES collaboration has also measured the rapidity distribution of dielectrons. The results from the coarse-grained simulations as well as the data points are shown in Fig. 5 (f). The shape of the spectrum is reproduced well, but with some 20% excess above the data points which was already visible in the invariant mass spectrum. Note that the rapidity values are for the laboratory frame, i.e. for  $E_{\text{lab}} = 1.76 \text{ AGeV}$  mid-rapidity corresponds to a value of  $y_0 = 0.86$ .

## 2. DLS Results

Although the DLS measurement was done with a smaller acceptance and lower resolution than in the more recent analyses by the HADES Collaboration, it is nevertheless interesting to compare our results also with these heavy-ion data. The system Ca+Ca which was

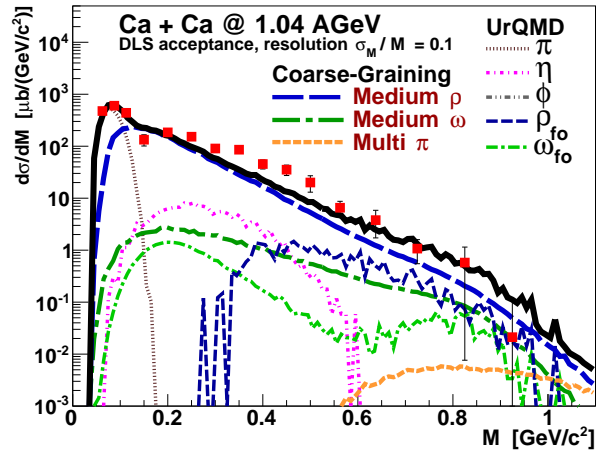


Figure 6. (Color online) Invariant-mass spectra of the dielectron yields for Ca+Ca collisions at  $E_{\text{lab}} = 1.04 \text{ AGeV}$  within the experimental acceptance. The results are compared to the data from the DLS Collaboration [19].

measured by DLS is comparable to the Ar+KCl reaction, as mentioned above. However, the DLS Collaboration performed the measurement at a lower energy of  $E_{\text{lab}} = 1.04 \text{ AGeV}$ . In Fig. 6 the coarse-grained UrQMD results for the according invariant-mass spectrum is shown within the DLS acceptance, together with the experimental data points [19]. In general the spectrum does not differ strongly from the simulations for HADES, but the peaks – especially in case of the  $\omega$  – are more smeared out here, which is due to the low mass resolution of only  $\sigma_M/M = 10\%$  of the detector, and the acceptance at low masses is suppressed compared to the HADES measurements. (For comparison, the mass resolution of the HADES experiment is roughly 2% in the region of the  $\rho$  and  $\omega$  pole masses [30].) While the overall description of the experimental spectrum with the present model is relatively good, a slight excess of the data above our model curve is present in the mass range from 0.2 up to 0.6  $\text{GeV}/c^2$ . This is in contrast to the findings for the HADES case, where we could describe this mass region quite accurately.

What might be the reasons for this deviation? It is possible that at this very low energy other processes presently not considered in our model might become more dominant here, e.g., an explicit bremsstrahlung contribution (note, however, that some bremsstrahlung effects are already considered within the in-medium spectral functions). As it has been shown that the importance of bremsstrahlung contributions increases with decreasing collision energy, these effects might be more significant than in Ar+KCl reactions at the slightly higher energies used for the HADES experiment. Nevertheless, there are still uncertainties within the different model calculations for the bremsstrahlung contribution, differing by a factor 2–4 [81, 82]. A main problem here is the

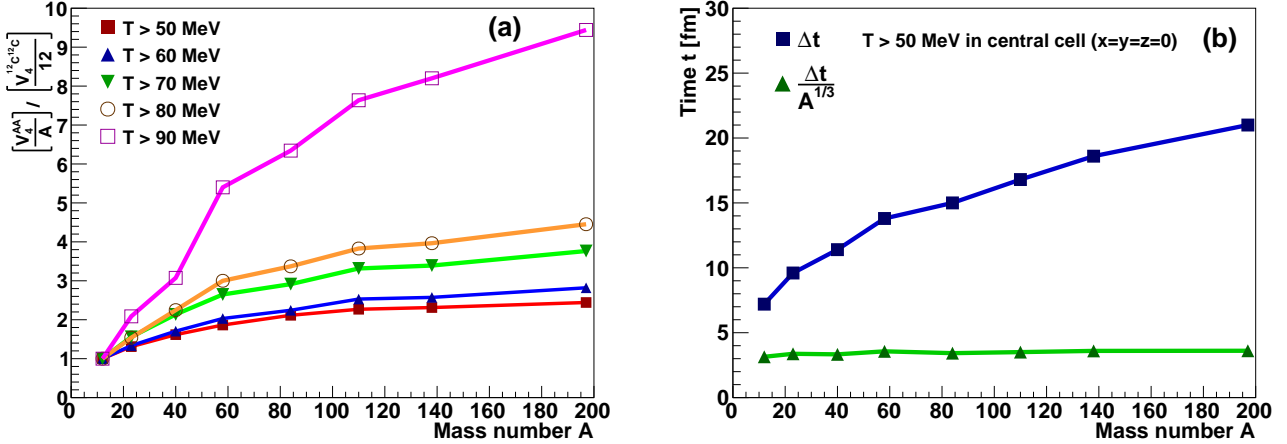


Figure 7. (Color online) (a) Ratio of the thermal four-volume  $V_4$  for different temperatures to the mass number  $A$  of the colliding nuclei. The results are normalized to the ratio obtained with  $^{12}\text{C} + ^{12}\text{C}$  collisions. (b) Time duration over which the central cell of the coarse-graining grid (for  $x = y = z = 0$ ) emits thermal dileptons, i.e., for this period of time the central cell has a temperature which is above 50 MeV (blue squares) and the same scaled by  $A^{1/3}$  (green triangles). Both plots (a) and (b) show the results in dependence on mass number  $A$  for central collisions and a collision energy  $E_{\text{lab}} = 1.76 \text{ AGeV}$ .

correct determination of the overall effect of the different interfering processes, which is highly non-trivial. The lower collision energy also results in slightly lower temperatures peaking around 80 MeV in general indicating less thermalization of the colliding system. Besides one has to take into account that the DLS experiment with its two-arm set-up had a more limited acceptance as compared to the HADES detector. This makes it difficult to draw clear quantitative conclusions from the comparison to the data. Additionally, the lack of a measured impact-parameter distribution hampers precise calculations within the coarse-graining approach, as the medium effects can be quite sensitive to the centrality of the collision.

However, it was shown (at least for C+C reactions) that the HADES results agree very well with those measured by the DLS collaboration if the HADES data are filtered with the DLS acceptance [21]. So these data should provide a good additional check for theoretical models in spite of their lower accuracy. Overall, the agreement is quite good especially considering that previous pure transport calculations with the UrQMD model (without bremsstrahlung) clearly underestimated the Ca+Ca data from DLS by a factor of 5-10 in the mass range from 0.2 to  $0.6 \text{ GeV}/c^2$  [72].

### C. System size and lifetime effects on thermal dilepton emission

The results of the previous section indicate that the size of the colliding nuclei (and in consequence also the size and duration of the hot and dense fireball created thereby) largely influence the thermal dilepton yield. This encourages a systematic study of the system size de-

pendence for thermal and non-thermal contributions and also raises the question, up to which point the assumption of a thermalized system seems reasonable. For this purpose we compare different systems from C+C to Au+Au in central collisions at an energy of  $E_{\text{lab}} = 1.76 \text{ AGeV}$ .

Fig. 7(a) shows the ratio of the thermal four-volume  $V_4$  for different temperatures to the mass number  $A$  of the colliding nuclei. The results are normalized to the ratio obtained with  $^{12}\text{C} + ^{12}\text{C}$  collisions. It is noteworthy here that the four-volume of the hottest cells ( $T > 90 \text{ MeV}$ ) shows a much stronger increase than the overall thermal volume (i.e., for  $T > 50 \text{ MeV}$ ). However, only the relative increase is shown in this plot. In direct comparison the number of cells with highest temperatures is very small compared to the total volume (approximately 1/30 for C+C). It is furthermore striking that the increase of the thermal four-volume is not proportional to  $A$ , but it shows a stronger increase for larger systems. This is not surprising, as  $A$  is only a measure for the volume of the colliding nuclei. In studies with the statistical model it was shown that at SIS energies the thermal freeze-out volume is closely related to the initial overlap volume of the system created in  $A - A$  collisions [73, 83]. However, the thermal four-volume is also determined by the lifetime of the fireball. As it is difficult to determine some kind of an average lifetime within the coarse-graining approach, we concentrate on the central cell of the grid and assume that the time for which it remains at an temperature greater than 50 MeV should be to first order a good approximation of the overall thermal lifetime. Fig. 7(b) shows the mentioned time duration over which the central cell emits thermal dileptons in dependence on  $A$ . Note that this duration approximately scales with  $A^{1/3}$ , i.e. with the diameter of the nuclei. Obviously the main influence on the lifetime at those low energies seems to

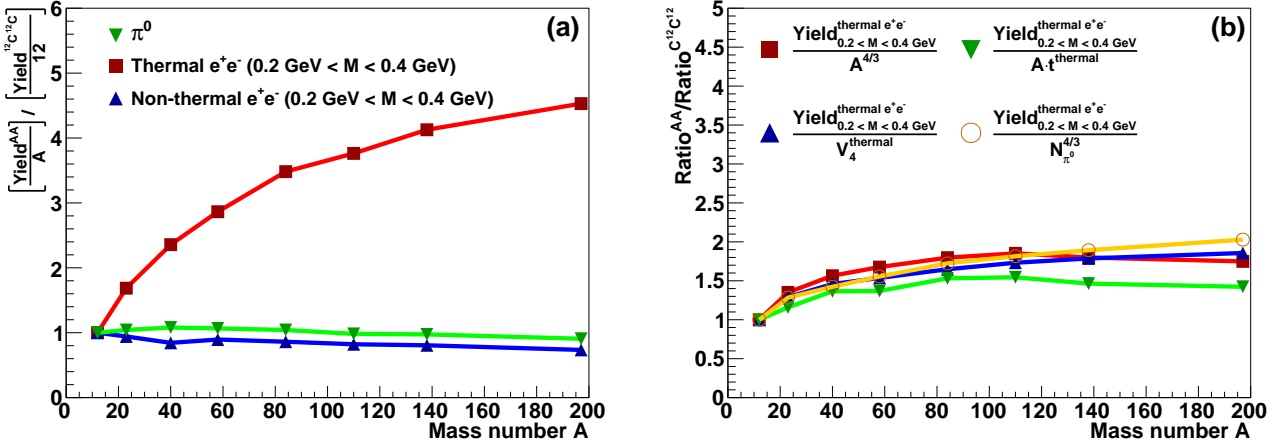


Figure 8. (Color online) (a) Ratio of the thermal (red squares) and non-thermal dilepton yield (blue triangles) in the invariant mass range from 0.2 to 0.4  $\text{GeV}/c^2$  to the mass number  $A$  of the colliding nuclei; the same ratio is plotted for the total number of  $\pi^0$  (green triangles). The results are normalized to the ratio obtained with  $^{12}\text{C} + ^{12}\text{C}$  collisions. (b) Ratio of the thermal dilepton yield in the invariant mass range from 0.2 to 0.4  $\text{GeV}/c^2$  in relation to  $A^{4/3}$  (red squares), to the thermal four-volume (blue triangles), the product of  $A$  and the time  $t^{\text{thermal}}$  in which the central cell (for  $x = y = z = 0$ ) emits thermal dileptons, i.e., is at  $T > 50 \text{ MeV}$  (green triangles) and the number of  $\pi^0$  produced in the reaction scaled with an exponent 4/3 (orange circles). All ratios are normalized to the result obtained for  $^{12}\text{C} + ^{12}\text{C}$ . Both plots (a) and (b) show the results for central collisions and a collision energy  $E_{\text{lab}} = 1.76 A \text{ GeV}$ .

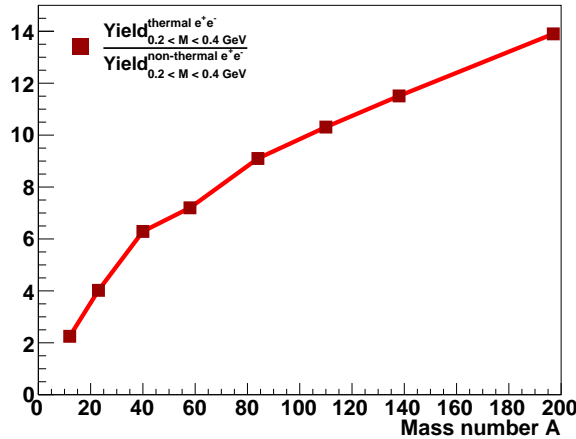


Figure 9. (Color online) Ratio of the thermal to the non-thermal dilepton yield in the mass range  $0.2 \text{ GeV}/c^2 < M_{ee} < 0.4 \text{ GeV}/c^2$  for  $A+A$  collisions at  $E_{\text{lab}} = 1.76 A \text{ GeV}$ . This ratio depicts the ‘excess’ of the thermal dilepton yield with regard to the cocktail contributions. The results are shown in dependence on the mass number  $A$  of the colliding nuclei.

be the time the two nuclei need to traverse each other.

The question now is which influence the evolution of the four-volume has on the production of lepton pairs. In Fig. 8 (a) the ratio of thermal and non-thermal dilepton yield as well as the total  $\pi^0$  yield in the invariant mass range from 0.2 to 0.4  $\text{GeV}/c^2$  in relation to the mass number  $A$  of the colliding nuclei is shown. The results

are – again – normalized to the ratio obtained with  $\text{C}+\text{C}$  collisions. While the ratio of the  $\pi^0$  number as well as the non-thermal dileptons to the mass number remains roughly 1 for all system sizes (i.e. the non-thermal dilepton and  $\pi^0$  yield increases linearly with  $A$ ), the thermal yield shows a significantly stronger increase. This finding is in line with the larger thermal excess found in our calculations in  $\text{Au}+\text{Au}$  compared to  $\text{Ar}+\text{KCl}$  reactions.

If one now compares the increase of the thermal yield with the corresponding total thermal four-volume (which is all cells with  $T > 50 \text{ MeV}$ ), as shown in Fig. 8 (b), the finding indicates that the ratio between both shows only a very slight increase and remains almost constant, independent of the system size. The same is found if one calculates the relation between the thermal yield and the product of  $A$  with the thermal lifetime of the central cell (compare Fig. 7 (b)) or directly looks at the ratio between the thermal dilepton yield and mass number  $A$  respectively the number of produced neutral pions  $N_{\pi^0}$  scaled by an exponent  $\alpha = 4/3$ . All those quantities give an approximate measure of the thermal four-volume at the low energies considered here. At higher collision energies as, e.g., obtained at the CERN SPS or at RHIC (where the whole fireball is more pion-dominated rather than baryon-dominated) one would still expect an increase with  $N_{\pi^0}^\alpha$ , but not any longer with  $A^\alpha$ . However, note that in these cases the nuclei will traverse each other much faster and one will also find a significant transverse expansion of the fireball, so that the diameter of the nuclei can no longer be considered as a rough measure of the lifetime; consequently the parameter  $\alpha$  might be different here. Nevertheless, in a different model calculation [44] it

was found that the thermal dilepton yield at top RHIC energy scales with the number of charged particles as  $N_{\text{ch}}^\alpha$ , where  $\alpha$  is found to take a value of approximately 1.45. This result is not so far from the value obtained within our simple picture – at a completely different energy regime.

In consequence, we learn from these results that the non-thermal dilepton contributions (from long-lived mesons as the  $\pi^0$  and the  $\eta$ , respectively from the freeze-out  $\rho$  and  $\omega$ ) increase with  $A$  and therefore directly with the volume of the colliding system. This is due to the fact that these contributions reflect the final hadronic composition, after the whole reaction dynamics has ended. Therefore the time-evolution of the system is irrelevant here. In contrast, the thermal dilepton emission does not only increase with the volume, but also with the time in which the colliding system remains in a hot and dense stage. This is obvious, as the thermally emitted dileptons will escape the fireball unscathed, while all hadronic particles undergo processes as rescattering and reabsorption. In consequence, the thermal yield increases roughly proportional to  $V \cdot \Delta t \sim A \cdot A^{1/3} = A^{4/3}$ . Exactly due to the different mechanisms for thermal and non-thermal dilepton contributions, one observes a significant increase of their ratio when going to larger system sizes. This ratio is shown (for the invariant mass range from 0.2 to  $0.4 \text{ GeV}/c^2$ ) in Fig. 9 with its value increasing from slightly over two for C+C up to 14 for Au+Au.

The present results qualitatively agree with a recent study on the same issue performed within different microscopic transport models, where the total dilepton yield was found not to scale with  $A$  or the number of neutral pions, but showing a stronger increase due to the complicated dynamics of the reaction [26]. There, from a microscopic point of view, it was also argued that the time evolution of the reaction is the main reason for the increasing dilepton yield in larger systems. If the dense phase with many binary scatterings lasts longer, according to this picture, a larger bremsstrahlung contribution (which is proportional to the number of collisions) and the repeated regeneration of  $\Delta$  resonances raises the dilepton yield. However, the contribution of other baryonic resonances was not explicitly considered there.

#### IV. CONCLUSIONS & OUTLOOK

We have presented results on dilepton production in Ar+KCl and Au+Au collisions at GSI SIS 18 and in Ca+Ca collisions at BEVALAC energies. The results are obtained using a coarse-grained microscopic transport approach and employing state-of-the-art spectral functions. With this approach the experimental dilepton spectra in heavy-ion collisions at  $E_{\text{lab}} = 1\text{-}2 \text{ AGeV}$  can be successfully described. The model represents a third way to explore the dynamics of heavy-ion reactions. In contrast to hydrodynamic/thermal fireball calculations or microscopic transport simulations it allows for a con-

sistent treatment of both, high-energy and low-energy collisions.

Our results show that the dominant in-medium effect, which is also visible in the dilepton spectra, stems from a strong broadening of the spectral shape of the  $\rho$  meson due to the high baryon density in the fireball. This causes a melting of the  $\rho$  peak and results in an enormous increase of the dilepton production below the pole mass. The reason for this is mainly the interaction with the baryonic resonances, especially the  $\Delta$  and  $N_{1520}^*$ , which are included in the spectral function and give significant additional strength to the  $\rho$  contribution at these low masses. The effect is much stronger at SIS energies than for RHIC or SPS. Here, the baryon-chemical potential remains very high for a significant time. This is visible in the dilepton spectra which always represent a four-volume integral over the whole space-time evolution. In the present study we also find a significant broadening of the  $\omega$  meson already at SIS energies.

Furthermore, the influence of the size of the colliding system on the thermal dilepton yield was studied. While we find the non-thermal contribution in the mass range from 0.2 to  $0.4 \text{ GeV}/c^2$  (which stems mainly from the long-lived  $\eta$ -meson but also from the “freeze-out”  $\rho$  and  $\omega$ ) to scale linearly with the mass number  $A$ , a stronger increase of the thermal  $\rho$  and  $\omega$  yield is observed. Their contribution to the dilepton yield scales with  $A t^{\text{thermal}}$ , i.e., the system’s volume multiplied with the lifetime of the thermal stage. Since  $t^{\text{thermal}}$  increases with the diameter of the nuclei which is proportional to  $A^{1/3}$ , we argue that the thermal dilepton emission should scale with  $A^{4/3}$ . As the number of neutral pions directly scales with  $A$ , we find the thermal dilepton yield also increasing with  $N_{\pi^0}^{4/3}$ . For future studies it might be quite instructive to check whether this proportionality still holds for higher collision energies.

It is interesting to compare our findings with the results of pure transport calculations. There, in recent calculations the dilepton excess in the invariant-mass spectra above the cocktail were mainly explained by two different effects: (i) Bremsstrahlung contributions and (ii) Dalitz decays of baryonic resonances [26, 29]. It is important to understand that both effects are also included in the spectral functions applied here. These processes, as implemented in the transport models, correspond to cuts of the in-medium self-energy diagrams of the  $\rho$  meson. For example, a contribution to the self-energy from a  $\Delta$ -hole excitation would be represented in the transport model by the process  $\Delta \rightarrow \rho N \rightarrow \gamma^* N$ , assuming strict vector meson dominance. However, due to the completely different character of the approaches it is difficult to compare the single contributions quantitatively. Also note that the self-energies in hadronic many-body quantum-field theory approach correspond to a *coherent* superposition of the various scattering processes, while in transport approaches naturally the various processes are summed *incoherently*. A future detailed analysis of the self-energy contributions and their relative strengths might be fruit-

ful to better understand how far the both approaches, i.e., the transport (kinetic) and the equilibrium thermal quantum-field theory description of the dilepton-emission rates at such low energies agree. One should keep in mind that the same microscopic scattering and decay processes are underlying both approaches.

Apart from this, the main outcome of the present investigation is the possibility of a consistent description of dilepton production from SPS down to SIS energies within the same model. In both energy regimes the spectra can be described reasonably well by the assumption of medium modifications of the vector mesons' spectral properties, whereby the  $\rho$  plays the most significant role.

In the future, the CBM experiment at FAIR will offer the possibility to study medium effects in a collision-energy range, where this kind of study has not been carried out yet. With high (net-)baryon densities but also temperatures reaching up to or above the critical temperature  $T_c$ , this will be a further test for the spectral functions and theoretical models. Besides, the high lumi-

nosities expected at FAIR might enable to perform more detailed and systematic studies, as, e.g., the effect of various different system sizes on the dilepton yield or a study for different centralities, to obtain more information on the evolution of the reaction dynamics.

## ACKNOWLEDGEMENTS

The authors thank the HADES Collaboration and especially Tetyana Galatyuk for providing the acceptance filters and experimental data. Furthermore, we acknowledge Ralf Rapp for providing the parametrization of the spectral functions and many fruitful discussions. This work was supported by the Bundesministerium für Bildung und Forschung, Germany (BMBF), the Hessian Initiative for Excellence (LOEWE) through the Helmholtz International Center for FAIR (HIC for FAIR) and the Helmholtz Association through the Helmholtz Research School for Quark-Matter Studies (H-QM).

---

[1] E. L. Feinberg, *Nuovo Cim. A* **34**, 391 (1976).  
 [2] E. V. Shuryak, *Phys. Lett. B* **78**, 150 (1978).  
 [3] C. Gale and J. I. Kapusta, *Phys. Rev. C* **35**, 2107 (1987).  
 [4] C. Gale and J. I. Kapusta, *Nucl. Phys. A* **495**, 423C (1989).  
 [5] T. Hatsuda and S. H. Lee, *Phys. Rev. C* **46**, 34 (1992).  
 [6] F. Klingl, N. Kaiser, and W. Weise, *Nucl. Phys. A* **624**, 527 (1997).  
 [7] R. Rapp and J. Wambach, *Adv. Nucl. Phys.* **25**, 1 (2000).  
 [8] S. Leupold, V. Metag, and U. Mosel, *Int. J. Mod. Phys. E* **19**, 147 (2010).  
 [9] R. D. Pisarski, *Phys. Lett. B* **110**, 155 (1982).  
 [10] G. Brown and M. Rho, *Phys. Rept.* **363**, 85 (2002).  
 [11] R. Arnaldi et al. (NA60 Collaboration), *Phys. Rev. Lett.* **96**, 162302 (2006).  
 [12] G. Agakichiev et al. (CERES Collaboration), *Phys. Rev. Lett.* **75**, 1272 (1995).  
 [13] H. van Hees and R. Rapp, *Phys. Rev. Lett.* **97**, 102301 (2006).  
 [14] H. van Hees and R. Rapp, *Nucl. Phys. A* **806**, 339 (2008).  
 [15] K. Dusling, D. Teaney, and I. Zahed, *Phys. Rev. C* **75**, 024908 (2007).  
 [16] S. Endres, H. van Hees, J. Weil, and M. Bleicher (2014), arXiv: 1412.1965 [nucl-th].  
 [17] L. Adamczyk et al. (STAR Collaboration), *Phys. Rev. Lett.* **113**, 022301 (2014).  
 [18] F. Geurts (STAR Collaboration), *J. Phys. Conf. Ser.* **458**, 012016 (2013).  
 [19] R. Porter et al. (DLS Collaboration), *Phys. Rev. Lett.* **79**, 1229 (1997).  
 [20] G. Agakichiev et al. (HADES Collaboration), *Phys. Rev. Lett.* **98**, 052302 (2007).  
 [21] G. Agakishiev et al. (HADES Collaboration), *Phys. Lett. B* **663**, 43 (2008).  
 [22] G. Agakishiev et al. (HADES Collaboration), *Phys. Lett. B* **690**, 118 (2010).  
 [23] G. Agakishiev et al. (HADES Collaboration), *Phys. Rev. C* **84**, 014902 (2011).  
 [24] E. Bratkovskaya and W. Cassing, *Nucl. Phys. A* **807**, 214 (2008).  
 [25] E. Bratkovskaya, W. Cassing, and O. Linnyk, *Phys. Lett. B* **670**, 428 (2009).  
 [26] E. Bratkovskaya, J. Aichelin, M. Thomere, S. Vogel, and M. Bleicher, *Phys. Rev. C* **87**, 064907 (2013).  
 [27] K. Schmidt, E. Santini, S. Vogel, C. Sturm, M. Bleicher, et al., *Phys. Rev. C* **79**, 064908 (2009).  
 [28] J. Weil, H. van Hees, and U. Mosel, *Eur. Phys. J. A* **48**, 111 (2012).  
 [29] J. Weil, S. Endres, H. van Hees, M. Bleicher, and U. Mosel (2014), arXiv: 1412.3733 [nucl-th].  
 [30] T. Galatyuk (HADES Collaboration), *Int. J. Mod. Phys. Conf. Ser.* **26**, 1460052 (2014).  
 [31] B. Schenke and C. Greiner, *Phys. Rev. C* **73**, 034909 (2006).  
 [32] B. Schenke and C. Greiner, *Phys. Rev. Lett.* **98**, 022301 (2007).  
 [33] B. Schenke and C. Greiner, *Nucl. Phys. A* **785**, 170 (2007).  
 [34] E. L. Bratkovskaya, W. Cassing, R. Rapp, and J. Wambach, *Nucl. Phys. A* **634**, 168 (1998).  
 [35] W. Cassing and E. Bratkovskaya, *Nucl. Phys. A* **831**, 215 (2009).  
 [36] H. Barz, B. Kämpfer, G. Wolf, and M. Zetenyi, *Open Nucl. Part. Phys. J.* **3**, 1 (2010).  
 [37] J. Weil, U. Mosel, and V. Metag, *Phys. Lett. B* **723**, 120 (2013).  
 [38] J. Ruppert, C. Gale, T. Renk, P. Lichard, and J. I. Kapusta, *Phys. Rev. Lett.* **100**, 162301 (2008).  
 [39] E. Santini, J. Steinheimer, M. Bleicher, and S. Schramm, *Phys. Rev. C* **84**, 014901 (2011).  
 [40] G. Vujanovic, C. Young, B. Schenke, R. Rapp, S. Jeon, et al., *Phys. Rev. C* **89**, 034904 (2014).  
 [41] P. Huovinen, M. Belkacem, P. J. Ellis, and J. I. Kapusta, *Phys. Rev. C* **66**, 014903 (2002).  
 [42] S. Endres, H. van Hees, J. Weil, and M. Bleicher, *J. Phys. Conf. Ser.* **599**, 012020 (2015).

- [43] S. Endres, H. van Hees, J. Weil, and M. Bleicher (2015), arXiv: 1502.01948 [nucl-th].
- [44] R. Rapp, Adv. High Energy Phys. **2013**, 148253 (2013).
- [45] S. A. Bass, M. Belkacem, M. Bleicher, M. Brandstetter, L. Bravina, et al., Prog. Part. Nucl. Phys. **41**, 255 (1998).
- [46] M. Bleicher, E. Zabrodin, C. Spieles, S. A. Bass, C. Ernst, et al., J. Phys. G **25**, 1859 (1999).
- [47] H. Petersen, J. Steinheimer, G. Burau, M. Bleicher, and H. Stöcker, Phys. Rev. C **78**, 044901 (2008).
- [48] <http://www.urqmd.org>.
- [49] C. Eckart, Phys. Rev. **58**, 919 (1940).
- [50] D. Zschiesche, G. Zeeb, and S. Schramm, J. Phys. G **34**, 1665 (2007).
- [51] L. Bravina, E. Zabrodin, M. I. Gorenstein, S. Bass, M. Belkacem, et al., Phys. Rev. C **60**, 024904 (1999).
- [52] L. Bravina, E. Zabrodin, M. I. Gorenstein, S. Bass, M. Belkacem, et al., Nucl. Phys. A **661**, 600 (1999).
- [53] W. Florkowski and R. Ryblewski, Phys. Rev. C **83**, 034907 (2011).
- [54] W. Florkowski, M. Martinez, R. Ryblewski, and M. Strickland, Nucl. Phys. A **904-905**, 803c (2013).
- [55] L. D. McLerran and T. Toimela, Phys. Rev. D **31**, 545 (1985).
- [56] D. Bandyopadhyay, M. Gorenstein, H. Stöcker, W. Greiner, and H. Sorge, Z. Phys. C **58**, 461 (1993).
- [57] H. Bebie, P. Gerber, J. Goity, and H. Leutwyler, Nucl. Phys. B **378**, 95 (1992).
- [58] M. Kataja and P. Ruuskanen, Phys. Lett. B **243**, 181 (1990).
- [59] R. Baier, M. Dirks, K. Redlich, and D. Schiff, Phys. Rev. D **56**, 2548 (1997).
- [60] R. Baier, M. Dirks, and K. Redlich, Acta Phys. Polon. B **28**, 2873 (1997).
- [61] V. L. Eletsky, M. Belkacem, P. Ellis, and J. I. Kapusta, Phys. Rev. C **64**, 035202 (2001).
- [62] R. Rapp, G. Chanfray, and J. Wambach, Nucl. Phys. A **617**, 472 (1997).
- [63] M. Urban, M. Buballa, R. Rapp, and J. Wambach, Nucl. Phys. A **641**, 433 (1998).
- [64] R. Rapp and J. Wambach, Eur. Phys. J. A **6**, 415 (1999).
- [65] R. Rapp and C. Gale, Phys. Rev. C **60**, 024903 (1999).
- [66] R. Rapp, Phys. Rev. C **63**, 054907 (2001).
- [67] M. Dey, V. Eletsky, and B. L. Ioffe, Phys. Lett. B **252**, 620 (1990).
- [68] L. G. Landsberg, Phys. Rept. **128**, 301 (1985).
- [69] G.-Q. Li, C. M. Ko, G. E. Brown, and H. Sorge, Nucl. Phys. A **611**, 539 (1996).
- [70] K. Olive et al. (Particle Data Group), Chin. Phys. C **38**, 090001 (2014).
- [71] U. W. Heinz and K. S. Lee, Nucl. Phys. A **544**, 503 (1992).
- [72] C. Ernst, S. Bass, M. Belkacem, H. Stöcker, and W. Greiner, Phys. Rev. C **58**, 447 (1998).
- [73] J. Cleymans, H. Oeschler, and K. Redlich, Phys. Rev. C **59**, 1663 (1999).
- [74] E. Bratkovskaya, W. Cassing, M. Effenberger, and U. Mosel, Nucl. Phys. A **653**, 301 (1999).
- [75] G. Agakishiev et al. (HADES Collaboration), Eur. Phys. J. A **47**, 21 (2011).
- [76] T. Galatyuk (2014), private communication.
- [77] <http://www-hades.gsi.de>.
- [78] [http://macdls.lbl.gov/DLS\\_WWW\\_Files/Filter\\_4.1/](http://macdls.lbl.gov/DLS_WWW_Files/Filter_4.1/).
- [79] J. Weil and U. Mosel, J. Phys. Conf. Ser. **426**, 012035 (2013).
- [80] S. Endres and M. Bleicher, J. Phys. Conf. Ser. **426**, 012033 (2013).
- [81] L. Kaptari and B. Kämpfer, Nucl. Phys. A **764**, 338 (2006).
- [82] R. Shyam and U. Mosel, Phys. Rev. C **82**, 062201 (2010).
- [83] P. Braun-Munzinger, K. Redlich, and J. Stachel, in R. C. Hwa and X.-N. Wang (eds.), *Quark-Gluon Plasma 3* (World Scientific, Singapore, 2004), arXiv: nucl-th/0304013.